Journal of Applied Physics

Efficient Cherenkov emission of broadband terahertz radiation from an ultrashort laser pulse in a sandwich structure with nonlinear core

Cite as: J. Appl. Phys. **104**, 093105 (2008); https://doi.org/10.1063/1.3005987
Submitted: 15 May 2008 • Accepted: 09 September 2008 • Published Online: 05 November 2008

S. B. Bodrov, M. I. Bakunov and M. Hangyo

Efficient Cherenkov emission of broadband terahertz radiation from an ultrashort laser pulse in a sandwich structure with nonlinear core

S. B. Bodrov,[1,2] M. I. Bakunov,[2,1,a)] and M. Hangyo[3]
[1]*Institute of Applied Physics, Russian Academy of Sciences, Nizhny Novgorod 603950, Russia*
[2]*University of Nizhny Novgorod, Nizhny Novgorod 603950, Russia*
[3]*Laser Terahertz Division, Institute of Laser Engineering, Osaka University, Osaka, Japan*

(Received 15 May 2008; accepted 9 September 2008; published online 5 November 2008)

A scheme for efficient generation of broadband terahertz radiation by a femtosecond laser pulse propagating in a planar sandwichlike structure is proposed. The structure consists of a thin nonlinear core cladded with prisms made of a material with low terahertz absorption. The focused into a line laser pulse propagates in the core as a leaky or waveguide mode and emits Cherenkov wedge of terahertz waves in the cladding. We developed a theory that describes terahertz generation in such a structure and calculated spatial distribution of the generated terahertz field, its energy spectrum and optical-to-terahertz conversion efficiency. The developed theory predicts the conversion efficiency of up to several percent in a 1 cm long and 1 cm wide Si–$LiNbO_3$–Si sandwich structure with a 20 μm thick nonlinear layer pumped by 8.5 μJ Ti:sapphire laser with pulse duration of 100 fs. © *2008 American Institute of Physics*. [DOI: 10.1063/1.3005987]

I. INTRODUCTION

Optical rectification of ultrashort laser pulses in electro-optic crystals is a proven way to generate both broad and narrow band terahertz radiation. In this technique, the pump optical pulse propagating through an electro-optic material produces a nonlinear polarization that follows the intensity envelope of the pulse. The nonlinear polarization moves with the group velocity of the optical pulse and emits terahertz radiation.

The efficiency of the optical-to-terahertz conversion is essentially affected by parameters of the electro-optic material, such as its nonlinear coefficient, velocity mismatch between the optical pulse and terahertz waves, optical transparency, and terahertz absorption. A variety of different materials have been tested for optical rectification of ultrashort laser pulses (see, for example, Refs. 1 and 2). All the materials have some advantages and disadvantages. For example, ZnTe provides phase matching of Ti:sapphire laser pulses (~800 nm wavelength) with a ~2.5 THz collinearly propagating wave. However, the nonlinear coefficient of ZnTe is not as high as in some other materials, such as $LiNbO_3$, $LiTaO_3$, or DAST.[3] Moreover, ZnTe suffers from relatively high terahertz absorption (~10 cm^{-1} at room temperature[4,5]) and strong two-photon absorption of the Ti:sapphire laser radiation at high laser intensities. These factors lead to saturation of terahertz yield at high laser intensities[6] and large crystal thicknesses,[7] therefore, the optical-to-terahertz conversion efficiency in ZnTe is typically lower than 10^{-6}–10^{-5}.

In the materials with higher optical nonlinearities and wider band gaps (smaller multiphoton absorption), such as $LiNbO_3$ or $LiTaO_3$, the optical group velocity is more than two times larger than the highest phase velocity of terahertz waves. Additionally, these materials have high terahertz absorption, especially at frequencies above 1 THz. For example, the intensity absorption coefficient of $LiNbO_3$ increases from about 16 cm^{-1} at 1 THz to more than 170 cm^{-1} at 2.5 THz at room temperature.[3,8] Despite the mentioned drawbacks, $LiNbO_3$ still remains an attractive material for optical rectification and different ways to overcome the limitations on the optical-to-terahertz conversion efficiency existing in $LiNbO_3$ and similar materials have been developed.

To compensate the velocity mismatch, a quasi-phase-matching schemes based on periodically poled lithium niobate (PPLN) structures were proposed.[9,10] Relatively high conversion efficiencies (10^{-5}) were reached for femtosecond pulses at 800 nm in a PPLN structure where the terahertz absorption was reduced by cryogenic cooling (18 K) of the structure.[11] To decrease the attenuation of the generated terahertz waves in a PPLN structure, surface emission schemes are developed.[10,12] In such a scheme, the generated terahertz wave is emitted through a lateral surface of the PPLN structure and, therefore, its propagation length in $LiNbO_3$ is minimized. Essentially, the quasi-phase-matching mechanism does not provide an increase in the generated terahertz power relative to the one from a single nonlinear slab. Using PPLN, however, enables one to increase the terahertz yield via generation of multicycle (narrow band) terahertz wave packets.

Another way to achieve phase matching in the materials, such as $LiNbO_3$, where the optical group velocity exceeds the phase velocity of terahertz waves (the so-called superluminal materials[7,13,14]) is to use pump pulses with tilted fronts.[15] The operation principle has been demonstrated by generating subpicosecond pulses at approximately 2 THz by Ti:sapphire laser pulses in $LiNbO_3$ with a conversion efficiency of 4.3×10^{-5} at 77 K.[16] In less absorbing $LiNbO_3$

a)Electronic mail: bakunov@rf.unn.ru.

crystal compositions, the efficiency was increased up to 1.7×10^{-4}.[3] Further improvement of the conversion efficiency up to record values of 5×10^{-4} and even 6×10^{-4} at room temperature was reported in Refs. 17 and 18. Recently, the technique was extended to the conversion of Yb-doped solid-state laser pulses (1035 nm wavelength) in $LiNbO_3$.[19] The drawback of using tilted-front pulses is that such pulses cannot propagate for a long distance because of significant diffractive distortions. This restricts the possible thickness of the nonlinear crystal by a few millimeters.

The most simple way to achieve phase matching in a superluminal material is the Cherenkov radiation mechanism.[20,21] To produce a Cherenkov cone of terahertz waves, the optical pulse should be focused to a size of the order of or smaller than the terahertz wavelength. Phase matching is achieved between the moving optical pulse and a plane terahertz wave propagating under a certain angle to the laser path. Due to dispersion, a continuum of plane waves with different frequencies and different propagating angles is excited by the pulse. If dispersion is negligible, all plane waves emitted from the laser pulse propagate at the same Cherenkov angle forming a shocklike wave. The generation of subpicosecond terahertz pulses via Cherenkov emission from a 60 fs laser pulse in $LiTaO_3$ was first demonstrated in Ref. 22, then this technique became standard for generating terahertz phonon polaritons in different crystals.[14,23,24] A theory of Cherenkov emission from ultrashort laser pulses in electro-optic crystals has been developing in Ref. 25 and later in Refs. 7 and 14.

A disadvantage of using Cherenkov radiation is the difficulty of extracting the terahertz pulses from the crystal due to total internal reflection. Typically large refractive index of the crystal at the terahertz frequencies leads to a small critical angle and the generated pulse suffers total internal reflection at the crystal boundary.[26] To overcome this limitation, a special shaping of crystals is used.[12,16,17] However, in the shaped crystal, the terahertz waves suffer strong attenuation while traveling from the point of generation to the output boundary of the crystal. Recently, it was proposed to put a silicon prism on the lateral surface of a $LiNbO_3$ crystal to output the Cherenkov radiation[27] (earlier, a Si-prism coupler was used to output the parametrically generated terahertz wave from a $LiNbO_3$ crystal[28]). The terahertz absorption in high-resistivity silicon is much lower than in $LiNbO_3$, and if the pump laser beam in $LiNbO_3$ is aligned parallel with and near the $LiNbO_3$-silicon interface, the propagation length of the terahertz radiation in $LiNbO_3$ is minimized. Moreover, the terahertz refractive index of silicon is intermediate between $LiNbO_3$ and air, therefore, the Cherenkov radiation can propagate through the $LiNbO_3$-silicon interface not experiencing the total internal reflection. In Ref. 27, using this scheme provided fivefold increase in the terahertz energy compared to the generation in the shaped $LiNbO_3$ crystal.

In this paper, we go further and propose to sandwich a thin layer of a nonlinear medium (for example, $LiNbO_3$) between two prisms (or a prism and substrate) made of a material (or materials) with low terahertz absorption (for example, high-resistivity Si). An advantage of such a structure is that it can constrain the pump laser pulse within the core providing its guiding for a long distance in the form of a waveguide or leaky mode (depending on the ratio of the optical refractive indices of the core and cladding). To input the laser pulse into the structure, we propose to focus it by a cylindrical lens onto the facet of the nonlinear core so that the light line would be parallel to the plane of the sandwich structure. Focusing the pump laser beam into a line can provide additional advantages for the construction of the powerful terahertz source. First, it prevents the laser pulse from the diffractive broadening in the plane of the structure, thus, increasing the efficient length of the structure. Second, in the case of focusing into a line, the terahertz pulse energy can be easily scaled up by using laser pulses with higher energy and increasing the length of the line in order to keep the optical intensity below the damage threshold of the nonlinear core. Third, the terahertz radiation emitted from the line source forms in the cladding the Cherenkov wedge, i.e., a beam having nearly flat phase front. This terahertz pattern is more convenient for practical applications as compared to the Cherenkov cone produced by the laser pulse focused to a spot. The line-source geometry of Cherenkov emission in a bulk electro-optic crystal was treated theoretically in Refs. 7 and 25 and was recently exploited for generation of terahertz pulses in $LiNbO_3$.[29]

Our generation scheme differs fundamentally from the recently proposed schemes with metal-dielectric[30,31] and C–GaAs–C (Ref. 32) planar waveguide structures. The above mentioned structures are designed to guide both the pump optical pulse and the generated terahertz wave and to provide phase matching between them. Due to the enhanced dispersion of guided terahertz waves, such schemes are aimed mostly at the generation of narrow band [for example, with the duration of ~30 ps (Ref. 32)] wave packets rather than broadband terahertz pulses.

The paper is organized as follows. In Sec. II, we describe the generation scheme and lay out the theoretical model and basic equations. The general solution of the equations for a generic sandwich structure by use of a Fourier-transform technique is given in Sec. III. In Sec. IV, we analyze the generated terahertz field, terahertz spectrum, and conversion efficiency for a specific $Si–LiNbO_3–Si$ structure pumped by Ti:sapphire laser (800 nm wavelength). In Appendix A, we give approximate formulas for the wave functions and propagation constants of the symmetric modes of an oversized dielectric slab waveguide. Optimal focusing of the pump laser beam is discussed in Appendix B. We estimate the radiative losses of a leaky mode of the dielectric slab waveguide in Appendix C and influence of the photoexcited carriers on the generated terahertz radiation in Appendix D.

II. GENERATION SCHEME AND THEORETICAL MODEL

The generation scheme is presented in Fig. 1. The sandwich structure consists of a planar core ($|x| < a/2$) made of a nonlinear material (for example, $LiNbO_3$) and two prisms ($|x| > a/2$) made of a material with low terahertz absorption (for example, Si). The thickness of the core a is assumed to be much greater than the optical wavelength and smaller than the terahertz wavelength ($a \sim 10–100$ μm). The facet of the

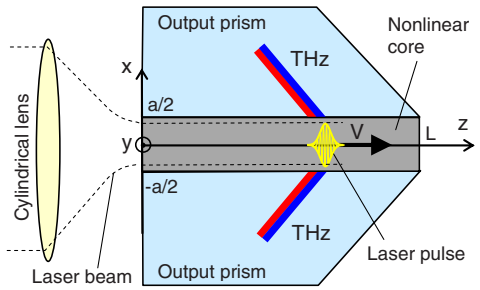

FIG. 1. (Color online) Generation scheme. An optical pulse focused to a line propagates in the nonlinear core of the sandwich structure and excites Cherenkov wedge of terahertz waves in the output prisms with low terahertz absorption.

core is illuminated normally by a femtosecond laser pulse focused in the x-direction by a cylindrical lens. The beam width in this direction $\ell_\perp$ can be varied to optimize the excitation of the fundamental mode of the slab waveguide (see Appendixes A and B). In the y-direction, the beam width is assumed to be much greater than the terahertz wavelength (of the order of several millimeters). This allows us to approximate it by a two-dimensional beam with fields independent of y.

We assume that, inside the sandwich, the laser pulse propagates in the $+z$-direction as the fundamental mode of the dielectric slab waveguide with a group velocity V, and we neglect the distortion of the pulse due to dispersion, linear absorption, and nonlinear effects, such as multiphoton absorption and self-focusing. The corresponding constraints on the distance z will be given further (Sec. IV). Since the waveguide is oversized, the fields of the optical pulse are localized predominantly within the core ($|x|<a/2$) and the group velocity V is defined practically only by the material dispersion of the core $V\approx c/n_g$, where n_g is the optical group refractive index of the core and c is the velocity of light (see Appendix A).

We approximate the transverse profile of the fundamental mode in the core of the oversized waveguide by the function $\propto\cos(\pi x/a)$ both in the case when the optical refractive index of the core n_c is greater than the optical refractive index of the prisms n_p, $n_c>n_p$, and in the opposite case $n_c<n_p$ (Appendix A). For $n_c>n_p$, the optical pulse propagates in the core as a waveguide mode and for $n_c<n_p$ as a leaky mode. The distances z, at which the radiative losses of the optical energy (for $n_c<n_p$) can be neglected, are estimated in Appendix C and Sec. IV. We do not account for the transient effects at the entrance ($z=0$) and exit ($z=L$) boundaries of the sandwich structure focusing on the stationary regime of terahertz emission in the infinitely long structure.

The above mentioned approximations allow us to treat the nonlinear polarization produced by the optical pulse in the core via nonlinear optical rectification as a function of two variables, x and $\xi=t-z/V$, i.e., $\mathbf{P}^{NL}=\mathbf{P}^{NL}(x,\xi)$. Evidently, the generated by the nonlinear polarization terahertz fields, electric $\mathbf{E}$ and magnetic $\mathbf{B}$, depend on the same variables, $\mathbf{E}(x,\xi)$ and $\mathbf{B}(x,\xi)$.

To account for the dispersion of the nonlinearity, we relate the nonlinear polarization to the optical pulse in the Fourier domain [ω is the Fourier variable (frequency), which corresponds to ξ, ~ will denote quantities in the Fourier domain],

$$\tilde{\mathbf{P}}^{NL}=\mathbf{p}(\omega)\tilde{F}(\omega)G(x), \tag{1}$$

where the function $G(x)$ follows the transverse profile of the optical intensity in the core. In our approximation, $G(x)=\cos^2(\pi x/a)$ for $|x|<a/2$ and $G(x)=0$ for $|x|>a/2$ due to linearity of the cladding. $\tilde{F}(\omega)$ is the Fourier transform of the time-dependent envelope of the optical intensity. To specify our final formulas, we will use the following Gaussian functions:

$$F(\xi)=e^{-\xi^2/\tau^2},\quad \tilde{F}(\omega)=(\tau/2\sqrt{\pi})e^{-\omega^2\tau^2/4}, \tag{2}$$

where τ is the pulse duration [the standard full width at half maximum (FWHM) is $\tau_{\mathrm{FWHM}}=2\sqrt{\ln 2}\tau$].

The absolute value of the amplitude vector $\mathbf{p}(\omega)$ can be written via the effective nonlinear coefficient $d_{\mathrm{eff}}(\omega)$ of the core's material and the peak amplitude of the optical field in the core E_0, $p(\omega)=d_{\mathrm{eff}}(\omega)E_0^2$. The orientation of the vector $\mathbf{p}$ is determined by the polarization of the optical beam and orientation of the crystallographic axes of the core. In our general analysis, we will include all the three following components: p_x, p_y, and p_z.

To find the terahertz radiation generated by the nonlinear polarization (1), we use Maxwell's equations written in the frequency domain,

$$\nabla_\omega\times\tilde{\mathbf{E}}=-\frac{i\omega}{c}\tilde{\mathbf{B}}, \tag{3a}$$

$$\nabla_\omega\times\tilde{\mathbf{B}}=\frac{i\omega}{c}\varepsilon\tilde{\mathbf{E}}+\frac{4\pi i\omega}{c}\tilde{\mathbf{P}}^{NL}, \tag{3b}$$

where the nabla operator ∇_ω has components $(\partial/\partial x,0,-i\omega V^{-1})$ and the complex dielectric function in the terahertz range $\varepsilon(\omega,x)$ is $\varepsilon_c(\omega)$ in the core ($|x|<a/2$) and $\varepsilon_p(\omega)$ in the prisms ($|x|>a/2$).

III. GENERAL SOLUTION FOR GENERIC SANDWICH STRUCTURE

Equations (3a) and (3b) projected into the coordinate system can be separated into two independent sets, for s-polarized waves (field components $\tilde{E}_y$, $\tilde{B}_x$, and $\tilde{B}_z$) and p-polarized waves (field components $\tilde{B}_y$, $\tilde{E}_x$, and $\tilde{E}_z$).

For s-polarized waves, eliminating $\tilde{B}_x$ and $\tilde{B}_z$ using

$$\tilde{B}_x=-n_g\tilde{E}_y,\quad \tilde{B}_z=-\frac{c}{i\omega}\frac{\partial\tilde{E}_y}{\partial x}, \tag{4}$$

we obtain an equation for $\tilde{E}_y$,

$$\frac{\partial^2\tilde{E}_y}{\partial x^2}+\kappa^2\tilde{E}_y=-\frac{4\pi\omega^2}{c^2}p_y\tilde{F}(\omega)G(x). \tag{5}$$

For p-polarized waves, eliminating $\tilde{E}_x$ and $\tilde{E}_z$ using

$$\tilde{E}_x=\frac{n_g}{\varepsilon}\tilde{B}_y-\frac{4\pi p_x}{\varepsilon}\tilde{F}G, \tag{6a}$$

$$\tilde{E}_z = \frac{c}{i\omega\varepsilon}\frac{\partial \tilde{B}_y}{\partial x} - \frac{4\pi p_z}{\varepsilon}\tilde{F}G, \tag{6b}$$

we obtain an equation for $\tilde{B}_y$,

$$\varepsilon\frac{\partial}{\partial x}\left(\frac{1}{\varepsilon}\frac{\partial \tilde{B}_y}{\partial x}\right) + \kappa^2\tilde{B}_y = -\frac{4\pi\omega^2}{c^2}\tilde{F}(\omega)\left\{p_x n_g G(x) - ip_z\frac{c\varepsilon}{\omega}\frac{\partial}{\partial x}\left[\frac{G(x)}{\varepsilon}\right]\right\}. \tag{7}$$

In Eqs. (5) and (7), we introduced the transverse wave vector $\kappa(\omega,x)$ given by

$$\kappa^2 = (\omega/c)^2[\varepsilon(\omega,x) - n_g^2]. \tag{8}$$

We proceed by solving Eqs. (5) and (7) in the homogeneous regions ($|x|<a/2$ and $|x|>a/2$) and matching the solutions by the boundary conditions of continuity $\tilde{E}_y$ and $\tilde{B}_z$ for s-polarized waves and $\tilde{B}_y$ and $\tilde{E}_z$ for p-polarized waves that arise after integrating Eqs. (5) and (7) across the boundaries at $x=\pm a/2$. We use also evenness of the function $G(x)$.

For s-polarized waves, we arrive at the following expressions for the electric field transform:

$$\tilde{E}_y = \begin{cases} C_1 e^{-i\kappa_p(x-a/2)}, & x > a/2 \\ C_2 e^{-i\kappa_c x} + C_3 e^{i\kappa_c x} + P(x), & |x| < a/2 \\ C_4 e^{i\kappa_p(x+a/2)}, & x < -a/2, \end{cases} \tag{9}$$

with

$$P(x) = \frac{2\pi\omega^2 p_y}{i\kappa_c c^2}\tilde{F}\int_{-a/2}^{a/2} dx' G(x') e^{-i\kappa_c|x-x'|}, \tag{10a}$$

$$C_2 = C_3 = C_1 e^{-i\kappa_c a/2}(1-\kappa_p/\kappa_c)/2, \tag{10b}$$

$$C_1 = C_4 = \frac{4\pi\omega^2 p_y}{ic^2\Lambda_s}\tilde{F}\int_{-a/2}^{a/2} dx G(x) e^{i\kappa_c x}, \tag{10c}$$

$$\Lambda_s = (\kappa_c+\kappa_p)e^{i\kappa_c a/2} - (\kappa_c-\kappa_p)e^{-i\kappa_c a/2}. \tag{10d}$$

The coefficient κ_p is κ taken with $\varepsilon=\varepsilon_p$ and κ_c is κ taken with $\varepsilon=\varepsilon_c$ [see Eq. (8)].

For p-polarized waves, we arrive at the following expressions for the magnetic field transform:

$$\tilde{B}_y = \begin{cases} D_1 e^{-i\kappa_p(x-a/2)}, & x > a/2 \\ D_2 e^{-i\kappa_c x} + D_3 e^{i\kappa_c x} + R(x), & |x| < a/2 \\ D_4 e^{i\kappa_p(x+a/2)}, & x < -a/2, \end{cases} \tag{11}$$

with

$$R(x) = \frac{2\pi\omega^2}{i\kappa_c c^2}\tilde{F}\int_{-a/2}^{a/2} dx'\left[p_x n_g G(x') - \frac{ip_z c}{\omega}G'(x')\right]e^{-i\kappa_c|x-x'|}, \tag{12a}$$

$$D_{2,3} = \left[\frac{D_{4,1}}{2}\left(1-\frac{\kappa_p\varepsilon_c}{\kappa_c\varepsilon_p}\right) \mp \frac{2\pi\omega p_z}{c\kappa_c}\tilde{F}G_0\right]e^{-i\kappa_c a/2}, \tag{12b}$$

$$D_{1,4} = \frac{4\pi\omega^2}{ic^2\varepsilon_c}\left[\frac{p_x n_g}{\Lambda_p^{(-)}} \mp \frac{p_z c\kappa_c}{\omega\Lambda_p^{(+)}}\right]\tilde{F}\int_{-a/2}^{a/2} dx G(x) e^{i\kappa_c x}, \tag{12c}$$

$$\Lambda_p^{(\pm)} = \left(\frac{\kappa_c}{\varepsilon_c}+\frac{\kappa_p}{\varepsilon_p}\right)e^{i\kappa_c a/2} \pm \left(\frac{\kappa_c}{\varepsilon_c}-\frac{\kappa_p}{\varepsilon_p}\right)e^{-i\kappa_c a/2}, \tag{12d}$$

where $G'(x')$ denotes the first derivative of $G(x')$ with respect to x' and $G_0 \equiv G(a/2)=G(-a/2)$ [$G_0=0$ in the approximation $G(x)=\cos^2(\pi x/a)$].

It follows from Eqs. (9) and (10c) that the emission of s-polarized waves to the prisms by the component p_y of the nonlinear polarization is symmetric, $C_1=C_4$. The p-polarized waves, according to Eqs. (11) and (12c), are emitted symmetrically ($D_1=D_4$) by the component p_x and antisymmetrically ($D_1=-D_4$) by the component p_z. The waves emitted by $p_{x,z}$ can interfere and produce an asymmetric radiation pattern.

With the solution in the Fourier-domain at hand (9)–(12), we can transform it to the ξ domain by taking the inverse transform in the form

$$E_y(\xi,x) = \int_{-\infty}^{\infty} d\omega \tilde{E}_y(\omega,x) e^{i\omega\xi}, \tag{13}$$

and the same formulas used for the other fields. Our numerical calculation of the radiation pattern for a specific sandwich structure in Sec. IV will be based on this formula.

To find the terahertz energy emitted to the prisms from the unit area of the core-prism interfaces, i.e., the terahertz fluence, we integrate the $\pm x$-components of the Poynting vector $S_{\pm x}=\pm(c/4\pi)E_y B_z$ and $S_{\pm x}=\mp(c/4\pi)E_z B_y$ for s- and p-polarization, respectively, at $x=\pm a/2$ over infinite interval $-\infty<\xi<\infty$. This yields the fluence for s and p polarizations in $\pm x$-directions,

$$W_{s,p}^{(\pm)} = \int_0^{\infty} d\omega w_{s,p}^{(\pm)}(\omega), \tag{14}$$

where $w_{s,p}^{(\pm)}(\omega)$ is the spectral density of fluence,

$$w_s^{(\pm)}(\omega) \equiv w_s(\omega) = c|C_1|^2 \mathrm{Re}(\varepsilon_p - n_g^2)^{1/2}, \tag{15a}$$

$$w_p^{(\pm)}(\omega) = c|D_{1,4}|^2 \mathrm{Re}[(\varepsilon_p - n_g^2)^{1/2}/\varepsilon_p]. \tag{15b}$$

The total terahertz fluence W is $W=2W_s+W_p^+ + W_p^-$.

It is instructive also to present W in a different form,

$$W = W_x + W_y + W_z, \tag{16}$$

where W_x, W_y, and W_z are the energies emitted by the p_x, p_y, and p_z components of the nonlinear polarization, respectively, i.e., $W_{x,z}=W_p^+ + W_p^-$ at $p_x\neq 0$, $p_z=0$ and $p_x=0$, $p_z\neq 0$, respectively, and $W_y=2W_s$. Equation (16) follows from Eqs. (12c), (14), and (15) and allows one to conclude that the interference between the waves emitted by p_x on one hand and p_z on the other hand does not change the total radiated energy but affects only the energy distribution between the upper ($x>a/2$) and lower ($x<-a/2$) prisms. Correspondingly, the spectral density of the total fluence $w(\omega)$ can be presented in the form $w(\omega)=w_x(\omega)+w_y(\omega)+w_z(\omega)$, where $w_{x,z}(\omega)=w_p^+(\omega)+w_p^-(\omega)$ at $p_x\neq 0$, $p_z=0$ and $p_x=0$, $p_z\neq 0$, respectively, and $w_y(\omega)=2w_s(\omega)$.

We introduce the optical-to-terahertz conversion efficiency per unit length of the sandwich structure (along the z-axis) as

$$\eta = W/W_{\text{opt}}, \tag{17}$$

where W_{opt} is the energy of the pump optical pulse per unit length along the y-axis. In the approximation that the optical intensity is negligible outside the core and has a profile $\propto\cos^2(\pi x/a)$ in the core and for the Gaussian time-dependent envelope (2), $W_{\text{opt}}=\pi^{1/2}I_0 a\tau/2$, where $I_0=(cn_c/8\pi)E_0^2$ is the peak optical intensity.

To get an analytical insight into the dependence of the generated terahertz spectrum and total terahertz energy on the parameters, we neglect at first the factors of terahertz dispersion and absorption, thus, considering ε_p and ε_c as real constants. We will also neglect here the dispersion of the nonlinearity assuming **p** to be frequency independent. For convenience of the analysis, we introduce the dimensionless parameters $\delta_c=|\varepsilon_c-n_g^2|^{1/2}$, $\delta_p=(\varepsilon_p-n_g^2)^{1/2}$, and $\sigma=\omega a\delta_c/(2\pi c)$. To provide the generation of Cherenkov radiation in the prisms by the laser pulse moving in the core, the condition $\varepsilon_p>n_g^2$ should be evidently fulfilled; ε_c and n_g^2 may be in an arbitrary ratio.

Substituting $G(x)=\cos^2(\pi x/a)$ and Gaussian time-dependent envelope (2) into Eqs. (10c) and (12c) and using Eqs. (15), we arrive at the following expression for the spectral density of fluence generated by the component p_j $(j=x,y,z)$ of the nonlinear polarization:

$$w_j(\sigma) = \frac{(2\pi c\tau)^2}{a} p_j^2 A_j \Phi_j(\sigma)\exp(-\sigma^2/\sigma_0^2), \tag{18}$$

where $\sigma_0=a\delta_c/(2^{1/2}\pi c\tau)$,

$$A_x = \frac{\varepsilon_p n_g^2}{\varepsilon_c^2\delta_p\delta_c^3}, \quad A_y = \frac{1}{\delta_p\delta_c^3}, A_z = \frac{\delta_p}{\varepsilon_p\delta_c^3}, \tag{19}$$

the function $\Phi_j(\sigma)$ is

$$\Phi_j(\sigma) = (1-\sigma^2)^{-2}[\gamma_j^2 + \cot^2(\pi\sigma)]^{-1}, \tag{20}$$

for $\varepsilon_c>n_g^2$, and

$$\Phi_j(\sigma) = (1+\sigma^2)^{-2}[\gamma_j^2 + \coth^2(\pi\sigma)]^{-1}, \tag{21}$$

for $\varepsilon_c<n_g^2$, with

$$\gamma_x = \gamma_z^{-1} = \varepsilon_p\delta_c/(\varepsilon_c\delta_p), \gamma_y = \delta_c/\delta_p. \tag{22}$$

In terms of the spectra $w_j(\sigma)$, the total terahertz fluence can be written in the form

$$W = \int_0^\infty d\sigma[w_x(\sigma) + w_y(\sigma) + w_z(\sigma)]. \tag{23}$$

According to Eq. (18), the spectral density $w_j(\sigma)$ is a product of two functions, Gaussian spectrum of the optical intensity envelope $\exp(-\sigma^2/\sigma_0^2)$ and the function $\Phi_j(\sigma)$. The function $\Phi_j(\sigma)$ (normalized to unity) is shown in Fig. 2 for two cases ($\varepsilon_c>n_g^2$ and $\varepsilon_c<n_g^2$) and three different values of the parameter γ_j. It is seen in Fig. 2 that for both cases and all the values of γ_j the function $\Phi_j(\sigma)$ is well localized within the interval $0<\sigma<2$. For $\varepsilon_c<n_g^2$ [Fig. 2(b)], the width of the function and position of its maximum only slightly depend on the parameter γ_j. For $\varepsilon_c>n_g^2$ [Fig. 2(a)], the effect of this parameter on the function's shape is more pronounced. The width of the function is maximal at $\gamma_j=1$ [solid line in Fig. 2(a)]. From the physical point of view, it is explained by the absence of reflection for the generated in the core terahertz waves at the core-prism boundaries under this condition. Indeed, according to Eq. (22), the condition $\gamma_j=1$ can be achieved in two cases. First, for any j (i.e., for arbitrary polarization of the terahertz waves) and equal dielectric constants of the core and the prisms, i.e., $\varepsilon_c=\varepsilon_p$, and, second, for $j=x,z$ at the condition $\varepsilon_c^{-1}+\varepsilon_p^{-1}=n_g^{-2}$ that corresponds to the incidence of a p-polarized wave on the core-prism boundary at the Brewster angle. Apparently, there is no reflection in both the cases. The function $\Phi_j(\sigma)$ becomes narrower as γ_j deviates from unity that can be explained by arising multiple reflections of the generated in the core terahertz waves from the core-prism boundaries. Indeed, the reflections make the transmitted to the prism terahertz pulse longer, thus, reducing the width of the pulse spectrum. It is also seen from Fig. 2(a) that for $\varepsilon_c>n_g^2$, γ_j significantly affects the position of the function's maximum. For $\gamma_j=1$, $\Phi_j(\sigma)$ is maximal at $\sigma=0.84$. For $\gamma_j>1$, the maximum shifts with γ_j to larger σ [dashed line, Fig. 2(a)] tending to $\sigma=1$ at $\gamma_j\to\infty$. For $\gamma_j<1$, the main peak of $\Phi_j(\sigma)$ shifts to smaller σ with decreasing γ_j and second peak appears [dotted line, Fig. 2(a)]. In the limit $\gamma_j\to 0$, the main peak tends to $\sigma=0.5$ and the second peak approaches $\sigma=1.5$.

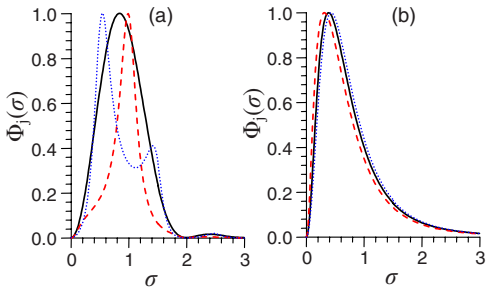

FIG. 2. (Color online) The function $\Phi_j(\sigma)$ (normalized to unity) in the cases (a) $\varepsilon_c>n_g^2$ and (b) $\varepsilon_c<n_g^2$ for different values of the parameter γ_j. $\gamma_j=1$ (solid line), $\gamma_j=0.5$ (dotted line), and $\gamma_j=2$ (dashed line).

For a short optical pulse with $\tau\ll a\delta_c/(9c)$, for which $\sigma_0\gg 2$, the Gaussian factor $\exp(-\sigma^2/\sigma_0^2)$ in Eq. (18) is close to unity in the whole interval $0<\sigma<2$, where the function $\Phi_j(\sigma)$ is not negligible. Thus, the generated spectrum $w_j(\sigma)$ is defined mainly by the function $\Phi_j(\sigma)$ rather than the Gaussian factor and, therefore, the terahertz fluence W is proportional to the integral of $\Phi_j(\sigma)$ over $0<\sigma<\infty$. We found numerically that this integral, as a function of γ_j, can be fitted with a high accuracy by the formula

$$\int_0^\infty d\sigma\Phi_j(\sigma) \approx \begin{cases} 2.47\gamma_j^{-1}, & \varepsilon_c > n_g^2 \\ 0.5(1+0.7\gamma_j^2)^{-1}, & \varepsilon_c < n_g^2. \end{cases} \tag{24}$$

Apparently, the integral (24) is larger at $\varepsilon_c>n_g^2$ than at $\varepsilon_c<n_g^2$ for any γ_j. Substituting the result of integration, for $\varepsilon_c>n_g^2$, from Eq. (24) into Eq. (23) and using Eqs. (18) and (19), we obtain the following expression for the total terahertz fluence in the case of short optical pulses:

$$W \approx \frac{9.9(\pi c\tau)^2}{a\delta_c^4}\left(\frac{n_g^2}{\varepsilon_c}p_x^2 + p_y^2 + \frac{\delta_c^2}{\varepsilon_c}p_z^2\right). \tag{25}$$

Four conclusions can be drawn from Eq. (25). First, the p_y component of the nonlinear polarization generates terahertz radiation more efficiently than other components ($n_g^2/\varepsilon_c < 1$ and $\delta_c^2/\varepsilon_c < 1$, for $\varepsilon_c > n_g^2$). Second, the terahertz yield does not depend on the dielectric constant of the prisms ε_p (ε_p should only exceed n_g^2 to satisfy the Cherenkov radiation condition). Third, W increases when ε_c approaches n_g^2 (δ_c decreases) and can even diverge, $W \to \infty$ at $\varepsilon_c \to n_g^2$, due to the contributions from p_x and p_y [the last term in Eq. (25) is limited from above by the applicability condition of the short pulse approximation]. Physically, the divergence of W can be explained by approaching the phase-matching condition for terahertz waves in the core at $\varepsilon_c \to n_g^2$. The similar effect was found for Cherenkov radiation in a homogeneous nondispersive medium.[7] It should be emphasized, however, to preserve the applicability of the short pulse approximation at $\varepsilon_c \to n_g^2$ the pulse duration τ should be simultaneously diminishing: $\tau \to 0$ (or $a \to \infty$). Fourth, for a fixed energy of the optical pulse, $p_j \tau a = \text{const}$ in Eq. (25) and thus $W \propto a^{-3}$. Correspondingly, the conversion efficiency (17) also scales as $\eta \propto a^{-3}$.

For a long optical pulse with $\tau \gg a\delta_c/(9c)$, for which $\sigma_0 \ll 2$, the width of the spectrum $w_j(\sigma)$ is limited by the Gaussian factor in Eq. (18) rather than the function $\Phi_j(\sigma)$. Taking into account that $\Phi_j(\sigma) \approx \pi^2\sigma^2$ for $\sigma \ll 1$ [see Eqs. (20) and (21)], we obtain $w_j(\sigma) \propto \sigma^2 \exp(-\sigma^2/\sigma_0^2)$. The spectrum $w_j(\sigma)$ has a maximum at $\sigma = \sigma_0$ ($\omega\tau = \sqrt{2}$). Evaluating integral (23) of this function $w_j(\sigma)$ we arrive at

$$W \approx \left(\frac{\pi}{2}\right)^{3/2}\frac{a^2}{c\tau\delta_p}\left(\frac{\varepsilon_p n_g^2}{\varepsilon_c^2}p_x^2 + p_y^2 + \frac{\delta_p^2}{\varepsilon_p}p_z^2\right). \tag{26}$$

According to Eq. (26), the p_x and p_y components of the nonlinear polarization are preferable for terahertz generation in the case of long optical pulses [$\delta_p^2/\varepsilon_p < 1$ in the last term of Eq. (26)]. Contrary to the limit of short optical pulses [Eq. (25)], W depends on ε_p. Dependence on ε_c enters only if $p_x \neq 0$. For a fixed energy of the optical pulse, $p_j \tau a = \text{const}$ in Eq. (26) and thus $W \propto \tau^{-3}$ (correspondingly, $\eta \propto \tau^{-3}$). Since τ is restricted from below in the long-pulse limit, increasing W (and the spectrum maximum frequency) via decreasing τ requires simultaneous decreasing the core thickness a.

In the general case of an arbitrary τ (arbitrary σ_0), the integral (23) of $w_j(\sigma)$ cannot be evaluated analytically. We evaluated this integral numerically and plotted W_j as a function of σ_0 for different values of γ_j in Fig. 3 [the curves have been normalized to unity by dividing them by the maximum value of $W_j(\sigma_0)$ at $\sigma_0 \to \infty$, which is given by a corresponding term in Eq. (25)]. It is seen from Fig. 3 that the function $W_j(\sigma_0)$ only slightly varies with changing γ_j in a wide interval. Therefore, to approximate the dependence $W_j(\sigma_0)$ analytically, we may restrict ourselves to the simple case when $\varepsilon_p = \varepsilon_c$ ($\gamma_j = 1$). Furthermore, we model the transverse profile of the nonlinear source $G(x) = \cos^2(\pi x/a)$, $-a/2 < x < a/2$ with a Gaussian function of very close shape, $G(x) = \exp(-16x^2/a^2)$, $-\infty < x < \infty$. After the above mentioned steps, we arrive at the well-studied case of Cherenkov radiation from a two-dimensional Gaussian laser pulse propagating in a homogeneous electro-optic medium.[7,25] According to the theory developed in Refs. 7 and 25, emitted by the pulse energy (per unit length of the linear laser pulse and unit length of the laser path) scales as $W \propto \tau^2\ell_\perp^2/[\tau^2 + (\varepsilon - n_g^2)\ell_\perp^2/c^2]^{3/2}$, where $\ell_\perp$ is the pulse width and ε is the dielectric constant of the medium in the terahertz range. Replacing $\ell_\perp \to a/4$ and $\varepsilon \to \varepsilon_c$, we obtain for the total terahertz fluence in our case,

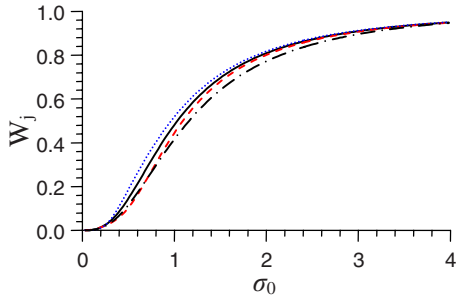

FIG. 3. (Color online) The terahertz fluence W_j (normalized to unity) as a function of σ_0 for $\gamma_j = 1$ (solid line), $\gamma_j = 0.5$ (dotted line), and $\gamma_j = 2$ (dashed line). The dashed-dotted line shows the function $W_j(\sigma_0)$ given by Eq. (27) [normalized by dividing by Eq. (25)].

$$W = \frac{\pi^{5/2}\tau^2 a^2}{8\sqrt{2}\delta_c c\tau_{\text{eff}}^3}\left(\frac{n_g^2}{\varepsilon_c}p_x^2 + p_y^2 + \frac{\delta_c^2}{\varepsilon_c}p_z^2\right), \tag{27}$$

where $\tau_{\text{eff}} = \sqrt{\tau^2 + (a\delta_c)^2/(4c)^2} = \tau\sqrt{1 + \pi^2\sigma_0^2/8}$. In the limit $\sigma_0 \gg 1$, Eq. (27) agrees with Eq. (25). In the opposite limit $\sigma_0 \ll 1$, Eq. (27) does not coincide completely with Eq. (26) (the difference between them depends on values of ε_c, ε_p, and n_g) but gives the same, as Eq. (26), dependence of the terahertz fluence on the parameters a and τ. In general, the dependence $W_j(\sigma_0)$ given by approximate Eq. (27), after the normalization to a corresponding term in Eq. (25), is independent of γ_j and differs insignificantly from the accurate curves $W_j(\sigma_0)$ in Fig. 3. An analytical formula (27) is convenient for estimating the terahertz fluence (see comparison with accurate calculations in Sec. IV) and allows us to introduce the optimal parameters of the laser pulse maximizing the terahertz yield or conversion efficiency.

For a fixed energy of the optical pulse, $p_j \tau a = \text{const}$ in Eq. (27) and $W \propto \tau_{\text{eff}}^{-3}$. Thus, for a given a, a decrease in τ leads to an increase in W; however, when τ becomes smaller than $\delta_c a/(4c)$, further shortening of the optical pulse adds little to the terahertz fluence. Similarly, for a given τ, a decrease in a (and, correspondingly, in the width of the laser beam illuminating the core's facet) leads to an increase in W until a becomes smaller than $4c\tau/\delta_c$.

If we fix the optical intensity rather than energy ($p_j = \text{const}$) and also fix a in Eq. (27), then $W \propto \tau^2/\tau_{\text{eff}}^3$ and an optimal pulse duration

$$\tau_W = a\delta_c/(2^{3/2}c) \approx 0.35a\delta_c/c \tag{28}$$

appears that maximizes W to a value $\propto a$. If we fix τ instead of a, then $W \propto a^2/\tau_{\text{eff}}^3$ and an optimal core thickness appears

$$a_W = 2^{5/2} c\tau/\delta_c \approx 5.7 c\tau/\delta_c \tag{29}$$

that maximizes W to a value $\propto \tau$. The optimal parameters (28) and (29) do not maximize, however, the conversion efficiency that, in the case of a fixed optical intensity, scales as $\eta \propto \tau a/\tau_{\text{eff}}^3$. To maximize η, one should use instead of (28) and (29) the following parameters, respectively:

$$\tau_\eta = a\delta_c/(2^{5/2}c) \approx 0.18 a\delta_c/c, \tag{30a}$$

$$a_\eta = 2^{3/2} c\tau/\delta_c \approx 2.8 c\tau/\delta_c. \tag{30b}$$

IV. TERAHERTZ GENERATION IN SI-LINBO$_3$-SI STRUCTURE

Let us now apply the general theory developed in Sec. III to a Si–$LiNbO_3$–Si structure pumped with Ti:sapphire laser (800 nm wavelength). Since the optical group refractive index of $LiNbO_3$, $n_g=2.23$ at 800 nm wavelength,[3] and the low-frequency dielectric constant of silicon, $\varepsilon_p=11.68$,[33] satisfy the condition $\varepsilon_p > n_g^2$, such a structure is appropriate for the generation of Cherenkov radiation in the Si-cladding by Ti:sapphire laser pulse propagating in the $LiNbO_3$-core. The optical refractive indices of the Si-cladding, $n_p \approx 3.67$,[34] and the $LiNbO_3$-core, $n_c=2.16$,[3] relates as $n_c < n_p$ at 800 nm wavelength, therefore, the optical pulse propagates in the structure as a leaky mode. Using Ti:sapphire laser for pumping the Si–$LiNbO_3$–Si structure has a drawback that the photon energy is larger than the band gap of silicon (1.1 eV, equivalent to 1.1 μm wavelength) and, consequently, photoexcitation of free carriers in Si near the Si–$LiNbO_3$ interface will occur. This can lead to undesirable additional absorption of the terahertz radiation by the photoexcited carriers. However, as we estimate in Appendix D, the effect of free carriers on the terahertz radiation is negligible for $W_{\text{opt}} < 40$ μJ/cm at $a \approx 10$ μm and even for higher W_{opt} at larger a. Moreover, it can be completely avoided by putting at the core-prism boundaries thin (compared to the terahertz wavelength) buffer layers of a material with a wide band gap and lower, than n_c, refractive index (for example, air).

In our calculations, we account for a small frequency-dependent terahertz absorption in high-resistivity silicon using the dielectric function $\varepsilon_p = 11.68 - i2\times 10^{-4}\nu$, where frequency ν is in terahertz, that was obtained by fitting the experimental data of Ref. 33. For $LiNbO_3$ at the terahertz frequencies, we use the experimental data of Ref. 8 for 0.68 mol % Mg-doped stoichiometric $LiNbO_3$ at room temperature. The experimentally measured frequency dependence of the amplitude absorption coefficient $\beta = (\omega/c)\text{Im}\sqrt{\varepsilon_c}$ given in Ref. 8 are fitted with a polynomial form $\beta[\text{cm}^{-1}] = 24.83 - 12.68\nu + 15.91\nu^2$, where ν is in terahertz. For the terahertz refractive index $n_{\text{THz}} = \text{Re}\sqrt{\varepsilon_c}$, we use the following fitting formula from Ref. 8: $n_{\text{THz}} = 4.94 + 2.1\times 10^{-2}\nu^2 + 1.2\times 10^{-3}\nu^4$ with ν in terahertz.

We assume that the optical axis of the $LiNbO_3$ core is along the y axis (Fig. 1), and the laser pulse is polarized along the optical axis and produces nonlinear polarization in the same direction with $p_y = d_{\text{eff}} E_0^2$, where $d_{\text{eff}} = d_{33}$. This geometry is optimal for the optical-to-terahertz conversion in the sandwich structure. According to Sec. III, the p_y component of the nonlinear polarization generates terahertz radiation more efficiently than other components, and p_y is maximal for this orientation. For the nonlinear coefficient d_{33}, we use the formula from a coupled electron-ion oscillator model,[35,36] $d_{33}(\text{pm/V}) = 25 + 158\times\left|1 - \omega^2/\omega_{\text{TO}}^2 - i\gamma\omega/\omega_{\text{TO}}^2\right|^{-1}$ with $\omega_{\text{TO}}(2\pi)^{-1} = 7.68$ THz and $\gamma(2\pi)^{-1} = 0.1$ THz.

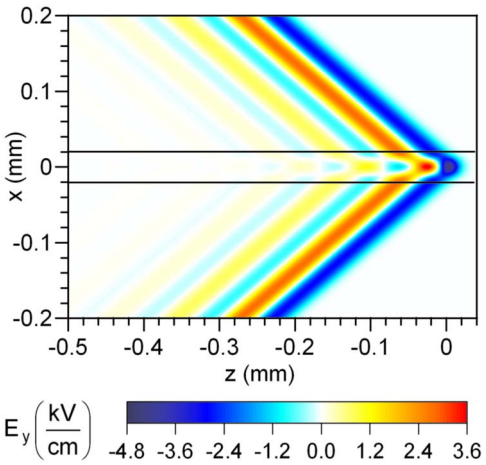

FIG. 4. (Color online) Snapshot of the electric field $E_y(x,z,t)$ at $t=0$ produced in a Si–$LiNbO_3$–Si structure with $a=40$ μm by a Ti:sapphire laser pulse with duration $\tau_{\text{FWHM}}=200$ fs and peak intensity $I_0=20$ GW/cm^2 ($W_{\text{opt}}=8.5$ μJ/cm). The Si–$LiNbO_3$ interfaces are shown with the horizontal lines.

Figure 4 shows the spatial distribution of the electric field E_y, calculated numerically on the basis of Eqs. (9), (10), and (13), for a Si–$LiNbO_3$–Si structure with $a=40$ μm. It is seen in Fig. 4 that the near field of the nonlinear source is localized well within the core and, therefore, the Cherenkov radiation in the prisms has its origin in the radiation generated in the core and then transmitted to the prisms through the core-prism interfaces. The opening angle of the Cherenkov cone in the prisms equals $\alpha_p \approx 41°$ in accord with theoretical formula $\sin\alpha_p = n_g/\varepsilon_p^{1/2}$.[7,21] The gradually fading oscillations in the field distribution across the Cherenkov cone can be attributed to multiple reflections of the generated in the core radiation at the core-prism interfaces. Such oscillations do not appear on the Cherenkov cone generated by a laser pulse in a homogeneous dispersionless (or weakly dispersive) medium.[7,25]

The spectral density of terahertz fluence $w(\omega)$, calculated using Eq. (15a), is shown in Fig. 5 for two core thicknesses and two laser pulse durations. Curve 1 in Fig. 5(a) and curves 1 and 2 in Fig. 5(b) are similar to the dimensionless function $\Phi_j(\sigma)$ with $\gamma_j=2$ in Fig. 2(a). It is in accord with our general theory (Sec. III). Indeed, $\varepsilon_c > n_g^2$ for the $LiNbO_3$ core ($\varepsilon_c \approx 25$, see the formula for n_{THz} above) like in Fig. 2(a). Then, $\sigma_0 > 1$ for the above mentioned curves [$\sigma_0 \approx 1.1$ for curve 1 in Fig. 5(a) and $\sigma_0 \approx 2.2$ and 1.1 for curves 1 and 2 in Fig. 5(b), respectively] and thus these curves are closely related to the limit of short laser pulses (see Sec. III), for which the Gaussian factor $\tilde{F}(\omega)$ (shown with dashed line in Fig. 5) is not essential and the spectrum's shape is determined mainly by the function $\Phi_j(\sigma)$. Furthermore, according to Eq. (22), $\gamma_y \approx 1.8$ for the Si–$LiNbO_3$–Si structure what is close to $\gamma_j=2$ in Fig. 2(a). Due to the similarity between the

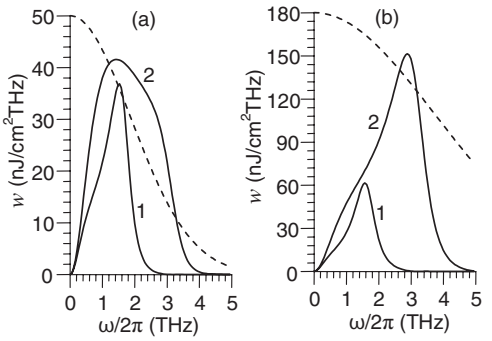

FIG. 5. The spectral density of terahertz fluence $w(\omega)$ generated by the optical pulse with (a) $\tau_{\mathrm{FWHM}}=200$ fs and (b) $\tau_{\mathrm{FWHM}}=100$ fs in the Si–$LiNbO_3$–Si structure with $a=40$ μm (curves 1) and $a=20$ μm (curves 2). The optical pulse energy (per unit length of the line source) is fixed to $W_{\mathrm{opt}}=8.5$ μJ/cm for all curves. The spectrum of the optical intensity envelope $\tilde{F}(\omega)$ is shown for corresponding τ_{FWHM} with the dashed line.

curves $w(\omega)$ and $\Phi_j(\sigma)$, the positions of the spectrum' maximums should be related to the peak of $\Phi_j(\sigma)$. The peak of $\Phi_j(\sigma)$ with $\gamma_j=2$ in Fig. 2(a) is at $\sigma\approx 0.9$ that corresponds, according to $\sigma=\omega a\delta_c/(2\pi c)$, to $\omega/(2\pi)\approx 1.5$ THz and 3 THz for the structure with $a=40$ μm and $a=20$ μm, respectively. This agrees well with the positions of the spectrum's maximum in Fig. 5(a) (curve 1) and Fig. 5(b) (curves 1 and 2). For curve 2 in Fig. 5(a), $\sigma_0\approx 0.55$ and, therefore (see Sec. III), the Gaussian factor $\tilde{F}(\omega)$ significantly affects the generated terahertz spectrum. This factor cuts the peak of the function $\Phi_j(\sigma)$ lying at $\omega/(2\pi)\approx 3$ THz what leads to broadening of the spectrum.

Let us now calculate the total terahertz fluence and optical-to-terahertz conversion efficiency for the Si–$LiNbO_3$–Si structure. Figures 6(a) and 6(b) show the conversion efficiency per unit length of the structure η, evaluated using Eqs. (14), (15a), and (17), as a function of a and τ_{FWHM} for a fixed energy of the optical pulse [Fig. 6(a)] and fixed optical intensity [Fig. 6(b)]. Figure 6(c) shows the total terahertz fluence $W=W_y$ as a function of the same variables for a fixed optical intensity. These figures agree well with the general theoretical predictions of Sec. III. For a fixed energy of the optical pulse [Fig. 6(a)], the efficiency increases with decreasing a and τ_{FWHM} in accord with Eqs. (25)–(27) and Fig. 3. For example, even for moderate parameters $a=20$ μm, $\tau_{\mathrm{FWHM}}=100$ fs, and $W_{\mathrm{opt}}=8.5$ μJ/cm ($I_0=80$ GW/cm^2), the efficiency can be as high as $\eta\approx 0.03$ cm^{-1}. This accurate value agrees well with the estimation given by the approximate analytical formula (27), $\eta\approx 0.04$ cm^{-1}. For a fixed optical intensity [Figs. 6(b) and 6(c)], there are optimal values of the parameters a (when τ is fixed) and τ (when a is fixed) maximizing η [Fig. 6(b)] or W [Fig. 6(c)], in accord with Eqs. (28), (29), (30a), and (30b). For example, for $\tau_{\mathrm{FWHM}}=200$ fs, Eq. (30b) predicts the optimal core thickness $a_\eta=24$ μm that agrees well with Fig. 6(b).

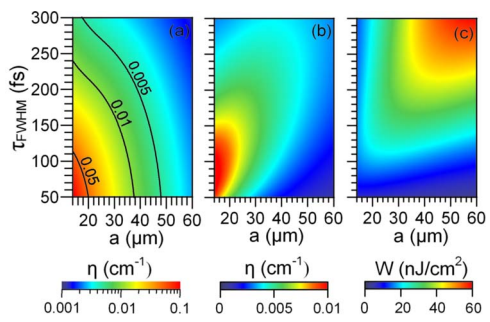

FIG. 6. (Color online) The conversion efficiency per unit length of the Si–$LiNbO_3$–Si structure η as a function of a and τ_{FWHM} for (a) the fixed optical pulse energy $W_{\mathrm{opt}}=8.5$ μJ/cm and (b) fixed optical intensity $I_0=20$ GW/cm^2. (c) The terahertz fluence W as a function of a and τ_{FWHM} for the fixed optical intensity $I_0=20$ GW/cm^2.

Up to now we considered the conversion efficiency per unit length (along the z axis) of the Si–$LiNbO_3$–Si structure. The total conversion efficiency for a structure of a finite length L can be approximately evaluated as ηL, neglecting the transient effects at the structure boundaries $z=0$ and $z=L$. Thus, the efficiency can be increased by using longer structures. There exist, however, some limitations from above on the structure length L. We mentioned these limitations earlier (see Sec. II), and now we specify them for the Si–$LiNbO_3$–Si structure. First, since the optical pulse of ~800 nm wavelength propagates in the Si–$LiNbO_3$–Si structure as a leaky mode ($n_c<n_p$), L is limited from above by the leakage length L_l introduced in Appendix C. For the fundamental mode of the Si–$LiNbO_3$–Si structure, the general expression for L_l given by Eq. (C1) can be reduced to a convenient for estimations form $L_l(\mathrm{cm})\approx 10^{-3}a^3$ with a in micrometers. For example, this formula gives $L_l\approx 64$ cm for $a=40$ μm and $L_l\approx 8$ cm for $a=20$ μm. Second, L should be smaller than the dispersion length, i.e., the length at which the dispersive broadening of the optical pulse becomes significant, $L_d=\tau^2/k_2$, where k_2 is the group velocity dispersion.[37,38] For $LiNbO_3$, $k_2\approx 370$ fs^2/mm,[39] and thus L_d can be written as $L_d(\mathrm{cm})\approx 10^{-4}\tau^2_{\mathrm{FWHM}}$ with τ_{FWHM} in femtosecond. For example, for typical pulse durations $\tau_{\mathrm{FWHM}}=200$ and 100 fs this formula gives $L_d\approx 4$ and ≈ 1 cm, respectively. Third, the nonlinear effects, such as self-focusing and filamentation, also impose limitations on the permissible length of the structure (according to our estimations, three-photon absorption in $LiNbO_3$ can be neglected for the intensities $I_0<100$ GW/cm^2 we consider here). Since the optical power P_{opt} in our examples significantly exceeds the critical power of self-focusing $P_{\mathrm{cr}}\approx 400$ kW for the beam of 800 nm wavelength in $LiNbO_3$ ($P_{\mathrm{opt}}/P_{\mathrm{cr}}\sim 200$ for $\tau_{\mathrm{FWHM}}=100$ fs and $W_{\mathrm{opt}}=8.5$ μJ/cm), we consider filamentation as a dominating factor. The filamentation length is $L_f=\lambda K/(2\pi n_2 I_0)$,[37] where $\lambda=800$ nm is the optical wavelength in vacuum, $n_2=9.5\times 10^{-16}$ cm^2/W is the nonlinear refractive index of $LiNbO_3$,[40] and K is a numerical factor of the order of 3–10. To find K, we refer to the experiment on terahertz generation in a 2 mm long $LiNbO_3$ crystal by focused to a line Ti:sapphire laser pulse.[17] In this experiment, the saturation of the generated terahertz energy at pump intensities of $I_0\approx 400$ GW/cm^2 was attributed to the development of filaments. It allows us to estimate the factor K as $K\approx 6$. Using this value of K, we arrive at formula $L_f(\mathrm{cm})\approx 80 I_0^{-1}$ with I_0 in GW/cm^2. For example, for $I_0=20$ GW/cm^2, this formula gives $L_f(\mathrm{cm})\approx 4$ cm. Depend-

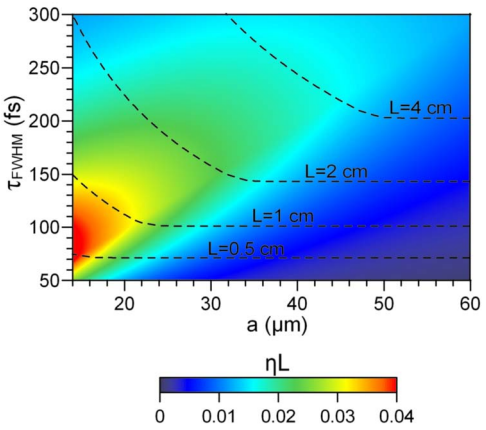

FIG. 7. (Color online) The conversion efficiency ηL for a Si–$LiNbO_3$–Si structure of a length $L=\min\{L_l, L_d, L_f\}$ as a function of a and τ_{FWHM}. Level curves of $L(a, \tau_{FWHM})$ are shown with dashed line. The optical pulse energy (per unit length of the line source) is fixed to $W_{opt}=8.5$ μJ/cm.

ing on the parameters a, τ_{FWHM}, and I_0, the permissible length L is limited by the minimum of the above-defined lengths L_l, L_d, or L_f.

Figure 7 shows the conversion efficiency ηL for a Si–$LiNbO_3$–Si structure of a maximal permissible length L as a function of a and τ_{FWHM} at a fixed optical pulse energy ($W_{opt}=8.5$ μJ/cm). For any a and τ_{FWHM}, L is taken as $L=\min\{L_l, L_d, L_f\}$, and therefore L is a function of a and τ_{FWHM}: $L=L(a, \tau_{FWHM})$ (level curves of L are shown with dashed line). In fact, for the range of parameters in Fig. 7, the leakage length L_l is always larger than L_d and L_f, and thus L equals the minimum of L_d and L_f, namely, $L=L_d(\tau_{FWHM})$ at the horizontal parts of the level curves and $L=L_f(a, \tau_{FWHM})$ at other parts of the curves. According to Fig. 7, for a given core thickness a, there is an optimal pulse duration τ_{FWHM} that maximizes the efficiency (and therefore the terahertz yield). For example, for $a=40$ μm, the maximum $\eta L \approx 0.02$ is achieved at $\tau_{FWHM} \approx 200$ fs (the corresponding structure length is $L \approx 3.5$ cm). Similarly, for a given τ_{FWHM} there is an optimal thickness a, for example, for $\tau_{FWHM}=150$ fs the maximum $\eta L \approx 0.03$ is achieved at $a \approx 18$ μm ($L \approx 1.3$ cm). The obtained above from Fig. 6(a) estimation $\eta=0.03$ cm^{-1} for $a=20$ μm and $\tau_{FWHM}=100$ fs corresponds almost exactly to the maximal length $L \approx 1$ cm in Fig. 7, thus giving $\eta L \approx 0.03$.

V. CONCLUSION

To conclude, we have shown that the Cherenkov emission of terahertz waves by optical rectification of the focused to a line femtosecond laser pulse propagating in a sandwich-like structure with thin nonlinear core and low absorbing cladding is a promising scheme for generating broadband terahertz radiation. This scheme offers a number of advantages. (i) The sandwich structure constrains the pump laser pulse within the core providing its guiding for a long distance and thus increasing the interaction length between the pulse and terahertz radiation. (ii) The propagation distance of the terahertz radiation within a typically strongly absorbing in the terahertz range nonlinear core is minimized. (iii) Focusing the pump laser beam into a line prevents its diffractive broadening in the plane of the structure, allows to scale up the terahertz energy, and forms more convenient for practical applications Cherenkov wedge, rather than Cherenkov cone. (iv) Properly cutting the cladding in the form of a prism provides efficient outcoupling of the terahertz radiation to vacuum.

We developed a theory that describes the optical-to-terahertz conversion in a generic sandwich structure. The theory allows one to calculate spatial distribution of the generated terahertz field, terahertz energy spectrum, and optical-to-terahertz conversion efficiency.

For Ti:sapphire laser, we proposed to use Si–$LiNbO_3$–Si structure. Applying the developed theory to such a structure, we predicted the conversion efficiency of up to 3% in a 1 cm long and 1 cm wide structure with a 20 μm thick core pumped by Ti:sapphire laser with $\approx$100 fs pulse duration and 8.5 μJ pulse energy (80 GW/cm^2 optical intensity). The frequency spectrum of the generated radiation spreads up to 4 THz with a maximum at about 3 THz.

Due to reduced effect of terahertz absorption in thin $LiNbO_3$ core on the terahertz generation, the structure can operate at room temperature, and the conversion efficiency should not be very sensitive to the composition (congruent or stoichiometric) or Mg-doping level of $LiNbO_3$. To suppress photorefraction in $LiNbO_3$, the doping level, however, should be above the photorefraction threshold, >0.6 mol % for stoichiometric and >5 mol % for congruent $LiNbO_3$.[41] Our consideration was restricted by moderate optical intensities $I_0 \lesssim 100$ GW/cm^2. To study how the terahertz yield saturates with further increasing the pump intensity (up to the optical damage threshold $\sim$1 TW/cm^2[17]), numerical modeling of the effect of filamentation and three-photon absorption on the terahertz generation is required.

ACKNOWLEDGMENTS

We are grateful to Dr. A. V. Maslov for fruitful discussions. Two of the authors (S.B.B. and M.I.B.) were supported in part by RFBR Grant Nos. 08-02-00988 and 08-02-92216 and RF President Grant No. MK-3749.2008.2. S.B.B. also acknowledges partial support from the fund "Dynasty." Part of this work has been supported by the Grant-in-Aid for Scientific Research from the Japanese Society of Promotion of Science.

APPENDIX A: APPROXIMATE SYMMETRIC MODES OF AN OVERSIZED DIELECTRIC SLAB WAVEGUIDE

In general, the transverse electric field (E_y or E_z for s- and p-polarized waves, respectively) of the symmetric modes of frequency Ω in a symmetric slab waveguide (Fig. 1) are described by the wave function of the form[42]

$$\psi(x) = \begin{cases} \cos(gx), & |x| < a/2 \\ \cos(ga/2)e^{-q(|x|-a/2)}, & |x| > a/2, \end{cases} \tag{A1}$$

where $g=(\Omega^2 n_c^2/c^2 - h^2)^{1/2}$, $q=(h^2 - n_p^2\Omega^2/c^2)^{1/2}$, and the propagation constant h is defined by the dispersion equation

$$g\tan(ga/2)=\begin{cases} q, & s\text{-modes} \\ q(n_c/n_p)^2, & p\text{-modes}. \end{cases} \tag{A2}$$

For $|n_c^2-n_p^2|(\Omega a/2c)^2 \gg 1$, the argument of the tangent in Eq. (A2) is close to $m\pi/2$, $m=1,3,5,\ldots$, $ga/2 \approx m\pi/2$,[42] and, therefore, the wave function (A1) can be approximately written as

$$\psi_m(x) \approx \begin{cases} \cos(m\pi x/a), & |x|<a/2 \\ 0, & |x|>a/2. \end{cases} \tag{A3}$$

The real and imaginary parts of the propagation constant $h_m=h_m'-ih_m''$ in this approximation are

$$h_m' \approx \frac{\Omega}{c}\mathrm{Re}\, n_c - \left(\frac{m\pi}{a}\right)^2 \frac{c}{2\Omega\, \mathrm{Re}\, n_c}, \tag{A4}$$

$$h_m'' \approx \frac{\Omega}{c}\mathrm{Im}\, n_c + \frac{(m\pi)^2}{a^3}\frac{2c^2}{\Omega^2\, \mathrm{Re}\, n_c} \times \begin{cases} \mathrm{Re}(n_p^2-n_c^2)^{-1/2}, & s\text{-modes} \\ \mathrm{Re}[n_p^2 n_c^{-2}(n_p^2-n_c^2)^{-1/2}], & p\text{-mode}. \end{cases} \tag{A5}$$

Essentially, this approximation is applicable to both the waveguide (at $\mathrm{Re}\, n_c > \mathrm{Re}\, n_p$) and leaky (at $\mathrm{Re}\, n_c < \mathrm{Re}\, n_p$) modes with not very high indices m.

In Eq. (A4), the first term describes the material dispersion of the core, while the second term describes the waveguide dispersion. In Eq. (A5), the first term defines the attenuation of the modes due to losses in the core, and the second term is related to the leakage of the electromagnetic energy from the core to the cladding (this term equals zero for real n_c, n_p and $n_c > n_p$).

APPENDIX B: OPTIMAL FOCUSING

An incident on the core facet laser pulse will excite, in general, a number of modes of the dielectric slab waveguide. Due to a difference in the modes' propagation constants h_m' [see Eq. (A4)], the modes will propagate with different group velocities what will lead to a distortion of the laser pulse in the course of its propagation along the sandwich structure. To avoid the distortion, one may try to adjust the width of the incident laser beam to excite predominantly a one of the modes.

To estimate the optimal beam width for the excitation of the fundamental mode (with $m=1$), we assume that the beam is incident normally on the facet $z=0$, the beam's waist coincides with the facet, and the optical field distribution along the x axis has a Gaussian profile at $z=0+$: $\psi_0(x) \propto \exp(-x^2/2\ell_\perp^2)$. Due to symmetry of the function $\psi_0(x)$, such a beam will excite only symmetric modes with odd values of m ($m=1,3,5,\ldots$). To find the mode amplitudes, we apply the standard technique of an arbitrary field expansion in a series of waveguide eigenmodes (neglecting the continuous radiation modes).[43] We write down $\psi_0(x)$ as a series of $\psi_m(x)$ with coefficients given by the overlap integrals of the product of $\psi_0(x)$ and $\psi_m(x)$ over the waveguide cross section. When evaluating the integral, we restrict the integration by the interval $-a/2<x<a/2$ thus neglecting the small modes' tails outside the waveguide core (see Appendix A) and periphery of the Gaussian beam (the beam's width is assumed to be smaller than the core thickness a).

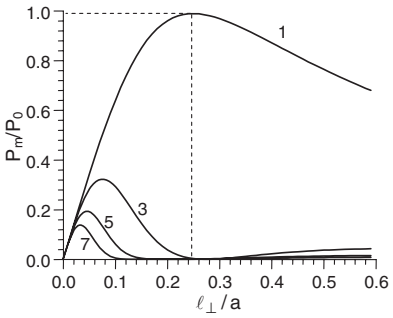

FIG. 8. The power of the mth mode (normalized to the power of the Gaussian beam P_0) as a function of the ratio $\ell_\perp/a$ for the first four symmetric modes with $m=1,3,5,7$ (shown near the corresponding curves).

Figure 8 shows the power of the mth mode P_m (normalized to the power of the Gaussian beam P_0 at $z=0+$) as a function of ratio $\ell_\perp/a$ for the first four symmetric modes ($m=1,3,5,7$). It follows from Fig. 8 that the maximal power of the fundamental mode $P_1/P_0=0.98$ is achieved at $\ell_\perp=0.25a$ when the modes with higher indices m are negligible. Practically, the beam width may be taken in the interval $\ell_\perp \approx (0.2-0.3)a$.

APPENDIX C: LEAKAGE LENGTH

Neglecting the material losses ($\mathrm{Im}\, n_c=\mathrm{Im}\, n_p=0$), we define the leakage length L_l of the mode (A1) at $n_c<n_p$ as the length at which the intensity of the leaky mode decreases by a factor of $\exp(-1)$: $L_l=(2\,\mathrm{Im}\, h)^{-1}$. Using approximation (A5), we obtain

$$L_l \approx \frac{a^3 n_c (n_p^2-n_c^2)^{1/2}}{\lambda^2 m^2} \times \begin{cases} 1, & s\text{-modes} \\ n_c^2 n_p^{-2}, & p\text{-modes}, \end{cases} \tag{C1}$$

where λ is the optical wavelength in vacuum. If n_c and n_p have small imaginary parts, Eq. (C1) still can be used after replacing n_c and n_p by their real parts. According to Eq. (C1), the fundamental mode (with $m=1$) has a maximal leakage length.

APPENDIX D: FREE CARRIER TERAHERTZ ABSORPTION

If the photon energy E_p of the pump laser is larger than the band gap E_g of the material the prisms are made of, an undesirable photoexcitation of free carriers in the prisms near the core-prism boundaries will occur. This can lead to additional reflection and absorption of the generated in the core terahertz radiation. To estimate the optical pulse energy, at which this effect becomes appreciable, we write the penetration depth of the laser light into the prism as $\Delta \sim \lambda/[4\pi\, \mathrm{Im}\sqrt{(n_p-i\alpha)^2-n_c^2}]$, where α is the extinction coefficient of the prism's material related to the photoexcitation. For the light of 800 nm wavelength in Si, $\alpha \approx 5\times 10^{-3}$ (Ref. 34) and $\Delta \sim 10$ μm. Then, we calculate the concentration of the photoexcited carriers N assuming the ionization process be one-photon and taking the optical energy leakage from the core to the prisms dW_{opt}/dz as $dW_{\mathrm{opt}}/dz \approx W_{\mathrm{opt}}/L_l$, where the

leakage length L_l is given by Eq. (C1). Thus, we arrive at $N \sim W_{\text{opt}}/(2\Delta L_l E_p)$. Further, we write the dielectric constant within the ionized layer using the Drude model $\varepsilon = \varepsilon_p - \omega_p^2/(\omega^2 - i\Gamma\omega)$, with $\omega_p = \sqrt{4\pi N e^2/m^*}$ as the plasma frequency, Γ is the collision frequency, e and m^* are the charge and effective mass of the free carriers, respectively. From the condition that the intensity of a generated terahertz wave of a frequency ω decreases by a factor of $\exp(-1)$ after transmission through the ionized layer, i.e., $2\omega\Delta\ \text{Im}\ \varepsilon^{1/2}/c \approx 1$, we evaluate ω_p and, finally, estimate the optical pulse energy,

$$W_{\text{opt}} \sim \omega_p^2 m^* \Delta L_l E_p/(2\pi e^2). \tag{D1}$$

For silicon [$E_g = 1.12$ eV, $m^* = 0.26 m_e$ with m_e the mass of free electron, and $\Gamma/(2\pi) \sim 1$ THz (Ref. 33)] excited with Ti:sapphire laser ($E_p = 1.55$ eV at $\lambda = 800$ nm), Eq. (D1) can be reduced, assuming $\omega/(2\pi) = 1$ THz and using Eq. (C1), to a convenient for estimations form $W_{\text{opt}}(\mu\text{J/cm}) \approx 0.04 a^3$ with a in micrometer. For example, the effect of free carriers on the terahertz radiation is negligible for $W_{\text{opt}} < 40\ \mu\text{J/cm}$ at $a = 10\ \mu\text{m}$.

[1] B. Ferguson and X.-C. Zhang, Nature Mater. **1**, 26 (2002).
[2] M. Tonouchi, Nat. Photonics **1**, 97 (2007).
[3] J. Hebling, A. G. Stepanov, G. Almási, B. Bartal, and J. Kuhl, Appl. Phys. B: Lasers Opt. **78**, 593 (2004).
[4] G. Gallot, J. Zhang, R. W. McGowan, T.-I. Jeon, and D. Grischkowsky, Appl. Phys. Lett. **74**, 3450 (1999).
[5] M. Schall, M. Walther, and P. U. Jepsen, Phys. Rev. B **64**, 094301 (2001).
[6] T. Loffler, T. Hahn, M. Thomson, F. Jacob, and H. G. Roskos, Opt. Express **13**, 5353 (2005).
[7] M. I. Bakunov, S. B. Bodrov, A. V. Maslov, and M. Hangyo, Phys. Rev. B **76**, 085346 (2007).
[8] L. Pálfalvi, J. Hebling, J. Kuhl, Á. Péter, and K. Polgár, J. Appl. Phys. **97**, 123505 (2005).
[9] Y.-S. Lee, T. Meade, V. Perlin, H. Winful, T. B. Norris, and A. Galvanauskas, Appl. Phys. Lett. **76**, 2505 (2000).
[10] C. Weiss, G. Torosyan, Y. Avetisyan, and R. Beigang, Opt. Lett. **26**, 563 (2001).
[11] Y.-S. Lee, T. Meade, M. DeCamp, H. Winful, T. B. Norris, and A. Galvanauskas, Appl. Phys. Lett. **77**, 1244 (2000).
[12] J. A. Lhuillier, G. Torosyan, M. Theuer, C. Rau, Y. Avetisyan, and R. Beigang, Appl. Phys. B: Lasers Opt. **86**, 185 (2007); **86**, 197 (2007).
[13] T. E. Stevens, J. K. Wahlstrand, J. Kuhl, and R. Merlin, Science **291**, 627 (2001).
[14] J. K. Wahlstrand and R. Merlin, Phys. Rev. B **68**, 054301 (2003).
[15] J. Hebling, G. Almási, I. Kozma, and J. Kuhl, Opt. Express **10**, 1161 (2002).
[16] A. G. Stepanov, J. Hebling, and J. Kuhl, Appl. Phys. Lett. **83**, 3000 (2003).
[17] A. G. Stepanov, J. Kuhl, I. Z. Kozma, E. Riedle, G. Almási, and J. Hebling, Opt. Express **13**, 5762 (2005).
[18] K.-L. Yeh, M. C. Hoffmann, J. Hebling, and K. A. Nelson, Appl. Phys. Lett. **90**, 171121 (2007).
[19] M. C. Hoffmann, K.-L. Yeh, J. Hebling, and K. A. Nelson, Opt. Express **15**, 11706 (2007).
[20] G. A. Askar'yan, Zh. Eksp. Teor. Fiz. **42**, 1360 (1962); [Sov. Phys. JETP **15**, 943 (1962)]; Phys. Rev. Lett. **57**, 2470 (1986).
[21] D. H. Auston, Appl. Phys. Lett. **43**, 713 (1983).
[22] D. H. Auston, K. P. Cheung, J. A. Valdmanis, and D. A. Kleinman, Phys. Rev. Lett. **53**, 1555 (1984).
[23] R. M. Koehl, S. Adachi, and K. A. Nelson, J. Phys. Chem. A **103**, 10260 (1999).
[24] N. S. Stoyanov, D. W. Ward, T. Feurer, and K. A. Nelson, Nature Mater. **1**, 95 (2002).
[25] D. A. Kleinman and D. H. Auston, IEEE J. Quantum Electron. **20**, 964 (1984).
[26] B. B. Hu, X.-C. Zhang, D. H. Auston, and P. R. Smith, Appl. Phys. Lett. **56**, 506 (1990).
[27] M. Theuer, G. Torosyan, C. Rau, R. Beigang, K. Maki, C. Otani, and K. Kawase, Appl. Phys. Lett. **88**, 071122 (2006).
[28] K. Kawase, M. Sato, K. Nakamura, T. Taniuchi, and H. Ito, Appl. Phys. Lett. **71**, 753 (1997).
[29] A. G. Stepanov, J. Hebling, and J. Kuhl, Appl. Phys. B: Lasers Opt. **81**, 23 (2005).
[30] H. Cao, R. A. Linke, and A. Nahata, Opt. Lett. **29**, 1751 (2004).
[31] R. R. Musin, Q. Xing, Y. Li, M. Hu, L. Chai, Q. Wang, Y. M. Mikhailova, M. M. Nazarov, A. P. Shkurinov, and A. M. Zheltikov, Appl. Opt. **47**, 489 (2008).
[32] V. A. Kukushkin, J. Opt. Soc. Am. B **23**, 2528 (2006).
[33] D. R. Grischkowsky, Opt. Photonics News **3**, 21 (1992).
[34] M. M. Koltun, in *Selective Optical Surfaces for Solar Energy Converters*, edited by D. P. Siddons (Allerton, New York, 1981).
[35] D. H. Auston and M. C. Nuss, IEEE J. Quantum Electron. **24**, 184 (1988).
[36] B. Bartal, I. Z. Kozma, A. G. Stepanov, G. Almási, J. Kuhl, E. Riedle, and J. Hebling, Appl. Phys. B: Lasers Opt. **86**, 419 (2007).
[37] R. W. Boyd, *Nonlinear Optics* (Academic, San Diego, 2003).
[38] S. A. Akhmanov, V. A. Vysloukh, and A. S. Chirkin, *Optics of Femtosecond Laser Pulses* (American Institute of Physics, New York, 1992).
[39] W. J. Tropf, M. E. Thomas, and T. J. Harris, in *Handbook of Optics*, edited by M. Bass (McGraw-Hill, New York, 1995), Vol. 2.
[40] R. DeSalvo, A. A. Said, D. J. Hagan, E. W. van Stryland, and M. Sheik-Bahae, IEEE J. Quantum Electron. **32**, 1324 (1996).
[41] L. Pálfalvi, J. Hebling, G. Almási, Á. Péter, K. Polgár, K. Lengyel, and R. Szipöcs, J. Appl. Phys. **95**, 902 (2004).
[42] H.-G. Unger, *Planar Optical Waveguides and Fibers* (Clarendon, Oxford, 1977).
[43] R. E. Collin, *Field Theory of Guided Waves*, 2nd ed. (IEEE, New York, 1990).